Asian Journal of Information Technology 15 (17): 3389-3397, 2016
ISSN: 1682-3915
© Medwell Journals, 2016

Biomedical Optical Image Classification for Glaucoma Using Wavelet Based Energy Features and FCM

G. Tamil Pavai
Department of Computer Science and Engineering,
Government College of Engineering, Tirunelveli, Tamil Nadu, India

Abstract: Glaucoma is the world's second largest reason for blindness worldwide as a results in the neuro degeneration of the optic nerve. The recovery of the degenerated optic nerve fibers is not medically feasible and Glaucoma is often undetected till its later stages. The objective of this study is to classify the given retinal image as Glaucoma image or healthy image using texture classification. Once the image is identified as a Glaucoma image, exudates are detected using Fuzzy c- means clustering. Texture classification plays a vital role in biomedical imaging, document processing, fault identification and other fields. For the past three decades, many models have been used for clinical image classification and identification or segmentation of abnormal tissues in the images. Texture features within images are actively pursued for accurate and efficient glaucoma classification. The R, G and B components of glaucoma images are considered as input for network formation. After that, the exudates are segmented in the given image.

Key words: Glaucoma, feature extraction, image segmentation, energy features, exudates

INTRODUCTION

Glaucoma is the world's second largest reason for blindness and results in the neuro degeneration of the optic nerve. The recovery of the degenerated optic nerve fibers is not medically feasible and Glaucoma is often undetected till its later stages. One medical survey estimates that approximately 11.1 million patients worldwide suffer from glaucoma induced bilateral blindness in 2020. Further in countries like India, it is estimated that approximately 11.2 million people over the age of 40 suffer from glaucoma. Fortunately, despite its severity, it is treatable disease if diagnosed at early stage. For the past decades, the Computer Aided Diagnosis (CAD) systems were used automation of disease identification and classification purposes. Most of the CAD systems were used various features such as color, texture and shape for feature extraction purpose.

Color and texture information are the fundamental characteristics of natural images. This information is important in visual perception. Texture patterns can be used in the analysis of images in several ways: in segmentation of scenes into distinct objects and regions in classification or recognition of surface materials and in computation of surface shape. Textures are replications, symmetries and combinations of various basic patterns or local functions, usually with some random variation. This means that they are particularly useful for searching visual databases and other human computer interaction applications. However, since, the notion of texture is spatial variations of intensity of color. Maenpaa et al. describes an algorithm for classifying color textures using wavelet transform for extracting features of images. A set of features are derived and combined for different color models. Arivazhagan *et al.* (2005) describes a set of features with color combination of features and for different color models, while the color information describes the first order properties of surfaces and scenes describes second order property are measured over image intensities. Lepisto *et al.* (2003) present an effective method for the classification of colored natural textures by multiresolution gabor filtering in color components of texture image.

Kandaswamy *et al.* (2012) propose a correlation-based transformation that minimizes the effect of illumination variation in color texture analysis. Carnapurn Wanderley and Fisher (2000) represent the color texture image is generated by decomposing each of three color channels of the image into several frequency, orientation and orientation bands using gabor filters and the author extract features from each color channel. The proposal of a new set of color texture affine and illumination invariants based on Human Visual System (HVS) are explained. Avia-Cervantes *et al.* (2007) presents on color texture histograms in the context of image interpretation and scene modeling. The proposed approach globally involved functions such as color segmentation, histogram texture analysis and region

recognition. Tan represent the use of three-dimensional color histograms by the product of three first-order histograms computed for the principal axis components of color image pixel data. Zheng *et al.* (2006) describes the color matching that combined with the characteristic of the light transmission, the image color matching based on two color space is compared and analyzed which are RGB color space and HSI color space. Kobayashi and Otsu (2009) proposed the color space and basic colors used for indexing colors by extracting color image features called color index local auto-correlations. Christodoulou *et al.* (2006) proposed the neural network Self-Organizing Feature Map (SOFM) classifier and the statistical K-Nearest Neighbour (KNN) classifier were used for the classification of the cloud images.

Ojala proposed outex framework contains a large collection of surface textures captured under different conditions which facilitates construction of a wide range of texture analysis problems. Liao *et al.* (2009) describes two sets of features: Dominant Local Binary Patterns (DLBP) in a texture image and the supplementary features extracted by using the circularly symmetric gabor filter responses. Bovik *et al.* (1990) proposed an encoding of images into multiple narrow spatial frequency by comparing the channel amplitude responses. Boundaries between textures can be detected by texture processing using a variety of real and synthetic textures. Chellappa and Chatterjee (1985) estimates Least Square (LS) of model parameters are used as features by using the notions of sufficient statistics including the origin are optimal feature for classification. Zhang *et al.* (2006) proposed a wide variety of distance functions applied to large, multiclass data sets for which it outperforms nearest neighbour and support vector machines, when problem becomes intractable for SVM, it becomes efficient. It permits recognition based on color, texture and particularly shape in a homogeneous framework.

Tamilpavai and Selvi (2012) discussed about the multiple representation of perceptual features. The authors considered the coarseness, busyness, directionality and contact for classification purpose. In their work 97% of classification rate were obtained for monochrome images. Several other methods also reported by researchers (Haralick *et al.*, 1973; Haralick, 1979; Kurmyshev and Yanez, 2005; Galloway, 1975; Yang *et al.*, 2012; Husoy *et al.*, 1993; Khellah, 2011) for texture classification. Artificial neural network techniques for segmentation of medical images are used by researchers (Zheng and Dong, 2013; Jiang *et al.*, 2010; Cheng *et al.*, 1999). Ahmed *et al.* (2011) suggests that Kullback-Leibler divergence measure for feature ranking and selection and the expectation maximization algorithm for feature fusion and tumor segmentation offer the best results for the patient data of their study. They used texture and intensity features for classification of medical images.

The goal of this paper is to develop an algorithm which automatically analyze eye ultrasound images and classify normal eye images and diseased glaucoma eye images. The two central issues are to automatic glaucoma recognition feature extraction from the retinal images and classification based on the chosen feature extracted.Features extracted from the images are categorized as either structural features or texture features. Here, Discrete Wavelet Transform (DWT) using daubechies wavelet, symlets wavelet and biorthogonal wavelet are used to extract features. Wavelet Energy signatures are calculated from these extracted features (Rajaei and Rangarajan, 2011). Probabilistic neural network is used to automatically analyse and classify the images as normal or abnormal eye images. Finally, this classifier can be used to distinguish between normal and glaucomatous images. We observed an accuracy of around 95%, this demonstrates the effectiveness of these methods. Then, exudates are detected using fuzzy c-means clustering of glaucoma images.

MATERIALS AND METHODS

Data set: The retinal images used for this study were collected from Digital Retinal Images for Vessel Extraction (DRIVE). DRIVE is a database which is having forty images. About 15 normal and 15 glaucoma images are taken from fundus image database. 130 images are collected from ophthalmologists. Totally 200 images of which 100 images for training and 100 images for testing purpose are considered for this study. Sample images of normal retinal and glaucoma images are shown in Fig. 1 and 2, respectively. Image classification is done in three steps:

- Image acquisition
- Feature extraction
- Image classification

Image acquisition: The first stage in fundal digital image analysis is image capture. This is normally acquired by a fundal camera (mydriatic or non-mydriatic) that has a back-mounted digital camera. Digital cameras use an image sensor like direct digital sensors are either a Charge-Coupled Device (CCD) or Complementary Metal Oxide Semiconductor Active Pixel Sensor (CMOS-APS) (Gonzalez and Woods, 2010).

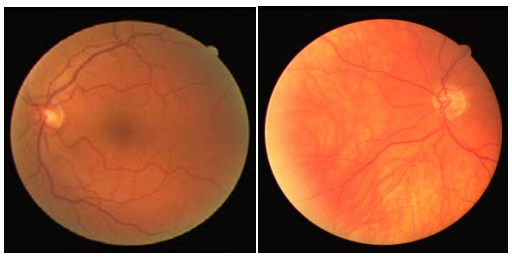

Fig. 1: Normal retinal images

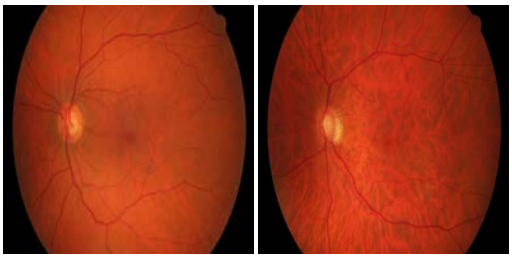

Fig. 2: Gluacoma retinal image

Lee *et al.* (2004) proposed an RNFL photographs were acquired by fundus camera system (CF-60UD, Canon Inc., Tokyo) integrated with digital camera (D60, Canon Inc.). Green filter was used to enhance the RNFL on the fundus photograph during acquisition. Image was stored in 1520×1080 pixel JPEG format for further analysis (Chandrika and Nirmala, 2013).

Feature extraction: Discrete wavelet transforms are implemented through sub-band coding. The DWT is useful in image processing because, it simultaneously localizes signals in time and scale. The 1-D DWT can be extended to 2-D transform using separable wavelet filters. With separable filters, applying a 1-D transform to all the rows of the input and the repeating on all of the columns can compute the 2-D transform. When one-level 2-D DWT is applied to an image, four transform coefficient sets are created. The four sets are LL, HL, LH and HH, where the first letter corresponds to applying either a low pass or high pass filter to the rows and the second letter refers to the filter applied to the columns. Three wavelet filters are used for extraction of texture features (Daubechies, 1988). The filters used in this work are as follows.

Daubechies transform: The daubechies wavelets are a family of orthogonal wavelets defining a discrete wavelet transform and characterized by a maximal number of vanishing moments for some given support. With each wavelet type of this class, there is a scaling function (called the father wavelet) which generates an orthogonal multi-resolution analysis. One of the daubechies wavelet used here is db3.

Symlets transform: The symlets are nearly symmetrical wavelets proposed by daubechies as modifications to the db family. Fourth-order symlets wavelet is used to extract features and analyze discontinuities and abrupt changes contained in signals.

Biorthogonal transform: Biorthogonal wavelets exhibit the property of linear phase which is needed for signal and image reconstruction. By using two wavelets, one for decomposition and the other for reconstruction instead of the same single one. Some of the bi-orthogonal wavelet used here is rbio3.3, 3.5 and 3.7.

Image classification: The energy obtained from the detailed coefficients can be used to distinguish between normal and glaucomatous images with very high accuracy. Hence, these energy features are highly discriminatory. This approach is very appealing due to its low computational complexity involving mainly the calculation of first and second order moments of coefficients.

Probabilistic Neural Network (PNN) is a feed forward network. It is designed from the Bayesian network and a algorithm called Kernal Fisher discriminant analysis. Probabilistic networks perform classification where the target variable is categorical.

Performance of the PNN classifier was evaluated in terms of training performance and classification accuracies. Probabilistic Neural Network gives fast and accurate classification and is a promising tool for classification of medical images. Existing weights will never be alternated but only new vectors are inserted into weight matrices when training. So, it can be used in real-time. Since, the training and running procedure can be implemented by matrix manipulation, the speed of PNN is very fast. The network classifies input vector into a specific class because that class has the maximum probability to be correct. In this research, the PNN has three layers: the input layer, radial basis layer and the competitive layer. Radial basis layer evaluates vector distances between input vector and row weight vectors in weight matrix. These distances are scaled by radial basis function nonlinearly. Competitive layer finds the shortest distance among them and thus finds the training pattern closest to the input pattern based on their distance.

Discussion for glaucoma image: This research investigates the discriminatory potential of wavelet features obtained from the daubechies (db3), symlets (sym3) and biorthogonal (bio3.3, 3.5 and 3.7) wavelet filters. A novel technique has been proposed to extract energy signatures obtained using 2-D discrete wavelet

transform and subject these signatures to different feature ranking and feature selection strategies. The developed model have gauged the effectiveness of the resultant ranked and selected subsets of features using a support vector machine, sequential minimal optimization, random forest and naive bayes classification strategies. It is observed that an accuracy of around 94.4% using tenfold cross validations to demonstrate the effectiveness of these methods.

This work proposes a glaucomatous image classification using texture features within images and it will be classified effectively based on feature ranking and neural network. In addition with, an efficient detection of exudates for retinal vasculature disorder analysis performed.The important texture features can be found by using the Energy distributions over wavelet subbands show in Eq. 1-3:

$$\text{Averag}\,Dh_1 = \frac{1}{p \times q}\Sigma_{x=\{p\}}\Sigma_{y=\{q\}}\left|Dh_1(x,y)\right| \quad (1)$$

$$\text{Averag}\,Dv_1 = \frac{1}{p \times q}\Sigma_{x=\{p\}}\Sigma_{y=\{q\}}\left|Dv_1(x,y)\right| \quad (2)$$

$$\text{Energy} = \frac{1}{p^2 \times q^2}\Sigma_{x=\{p\}}\Sigma_{y=\{q\}}\left(Dv_1(x,y)^2\right) \quad (3)$$

This system uses different wavelet features obtained from the daubechies (db3), symlets (sym3) and biorthogonal (bio3.3, 3.5 and 3.7) wavelet filters. The energy signatures obtained from 2-D discrete wavelet transform subjected to different feature ranking and feature selection strategies. The energy obtained from the detailed coefficients can be used to distinguish between normal and glaucomatous images with very high accuracy. This performance will be done by probilistic neural network model. The exudates are also detected effectively from the retina fundus image using segmentation algorithms.

RESULTS AND DISCUSSION

In research, 200 images are kept in dataset including normal and Glaucomatous defected abnormal images. Initially any one of the image from the test set is chosen to check whether it is normal or affected by Glaucoma. It undergoes preprocessing where decomposition using Discrete Wavelet transform is carried out. Wavelet filters such as Daubechies, Symlet, Bioorthogonal are used to extract energy signatures from it. The next step is to apply the filters to all training set and extract Energy signatures.

Then, the probabilistic neural network is used as a classifier that classifies the image in to one of the two classes, normal or abnormal. If the image results to abnormal, clustering using fuzzy c-means algorithm is used for exudates detection. The features extracted for various testing images are show in Table 1-5.

Figure 3a-i shows input image, gray scale image, daubachies wavelet, symlet, biorthogonal, abnormal detection 1, abnormal detection 2 and exudates detection, respectively for glaucoma affected image (Fig. 4).

Evaluation metrics: In this research, criteria including Similarity Index (SI), Overlap Fraction (OF) and Extra Fraction (EF) are used for evaluation. SI is a criterion for the correctly segmented region relative to the total segmented region in both the manual segmentation and the segmented image by the proposed method. The OF and the EF specify the areas that have been correctly and falsely classified images respectively. Similarity index, overlap fraction and extra fraction are obtained, respectively by Eq. 4-6:

$$SI = \frac{2TP}{2TP + FP + FN} \quad (4)$$

$$OF = \frac{TP}{TP + FN} \quad (5)$$

$$EF = \frac{FP}{TP + FN} \quad (6)$$

In these equations, TP is the number of true-positive pixels detected correctly by the method, FP is the number of false-positive pixels detected falsely by the method and FN is the number of false-negative pixels relative to the

Table 1: Texture feature values extracted for test image 1-4

Features	Test image 1	Test image 2	Test image 3	Test image 4
db3	0.168129622	0.052659508	0.110978131	-0.001720677
db3	12.380508470	89.929512330	39.928535700	652.597873900
sym3	0.168129622	0.052659508	0.110978131	-0.001720677
sym3	12.380508470	89.929512330	39.928535700	652.597873900
rbio3.3	0.169000880	0.052491079	-0.058937668	-0.003826653
rbio3.3	41.830815930	93.988050610	60.042011930	311.391400500
rbio3.3	3.028841287	24.493171480	4.895755511	7.452006170

Table 1: Continue

Features	Test image 1	Test image 2	Test image 3	Test image 4
rbio3.5	0.161489355	0.059817222	-4.31E-04000	-0.005070447
rbio3.5	30.643848810	93.553121280	222.297646400	444.802274900
rbio3.5	4.095013787	27.636728320	3.799977022	5.130055147
rbio3.7	0.176395572	0.026216710	-1.20E-05000	-0.003430901
rbio3.7	21.283919260	42.545207030	244.363192200	345.720896000
rbio3.7	6918.760959000	949.277102600	0.049374188	6.820763702
rbio3.7	4.095013787	27.636728320	3.799977022	5.130055147

Table 2: Texture feature values extracted for test image 5-8

Features	Test image 5	Test image 6	Test image 7	Test image 8
db3	0.013486956	-0.003472724	0.038003632	0.043220898
db3	107.059898200	15.885347210	9.663598703	177.834580300
sym3	0.013486956	-0.003472724	0.038003632	0.043220898
sym3	107.059898200	15.885347210	9.663598703	177.834580300
rbio3.3	0.009998408	-0.004623372	3.00E-16000	0.020502932
rbio3.3	114.369485900	479.781719100	6.659352022	58.151044060
rbio3.3	92.910882390	10.101615220	3.887655497	0.356170977
rbio3.5	0.006480239	-0.009229285	-0.009275279	0.017078956
rbio3.5	146.926644300	150.676248700	0.078957090	88.460383330
rbio3.5	86.310951380	9.440573300	5.074142157	0.204082414
rbio3.7	0.054755136	-0.009255431	-0.010224433	0.019208780
rbio3.7	87.231761950	224.981991000	0.023511832	75.320620800
rbio3.7	11.140960060	22.598346720	22.824142160	77.386131740
rbio3.7	86.310951380	9.440573300	5.074142157	0.204082414

Table 3: Texture feature values extracted for test image 9-12

Features	Test image 9	Test image 10	Test image 11	Test image 12
db3	0.010144808	-0.009228375	0.026822041	0.064980175
db3	27.746406670	6.152232468	3.894081034	178.508543400
sym3	0.010144808	-0.009228375	0.026822041	0.064980175
sym3	27.746406670	6.152232468	3.894081034	178.508543400
rbio3.3	0.007918379	7.44E-04000	0.031874009	0.066692723
rbio3.3	39.255119920	62.039373100	3.470427906	170.889252600
rbio3.3	9.428857096	7.762683560	8.527681614	16.976713640
rbio3.5	0.001781025	-6.36E-04000	0.032393453	0.065090744
rbio3.5	10.396350070	55.835661080	37.232360840	121.462433800
rbio3.5	11.732622930	9.383616728	8.236215629	16.606244260
rbio3.7	0.007136407	-0.001928094	0.041678177	0.025986959
rbio3.7	10.308862970	31.744970530	76.562430940	166.351246700
rbio3.7	0.841551318	0.107448241	278.390884600	1124.032831000
rbio3.7	11.732622930	9.383616728	8.236215629	16.606244260

Table 4: Texture feature values extracted for test image 13-16

Features	Test image 13	Test image 14	Test image 15	Test image 16
db3	0.068505908	-0.031101758	0.033891352	0.014816870
db3	12.145373870	33.674653330	131.400344500	639.915102600
sym3	0.068505908	-0.031101758	0.033891352	0.014816870
sym3	12.145373870	33.674653330	131.400344500	639.915102600
rbio3.3	0.071848868	-0.008535629	0.030722484	-0.014096141
rbio3.3	4.101277669	31.300896290	96.110984800	578.948989600
rbio3.3	0.212707030	33.833064730	1.994127796	1.611821773
rbio3.5	0.071147140	-0.018016471	0.101412974	-0.005087061
rbio3.5	2.870891880	23.361983730	16.715571520	607.576433100
rbio3.5	0.091950061	36.107575060	1.501378676	2.812538297
rbio3.7	0.071554292	-0.012325734	0.053666691	-0.020913342
rbio3.7	0.722851964	39.851942480	22.083937160	656.526914000
rbio3.7	1342.936311000	86.115227880	2728.522663000	6.865535100
rbio3.7	0.091950061	36.107575060	1.501378676	2.812538297

Table 5: Texture feature values extracted for test image 17-20

Features	Test image 17	Test image 18	Test image 19	Test image 20
db3	-0.031432100	-0.024985466	0.018225350	0.003108674
db3	1342.910204000	1.777957700	576.559067600	1.678590945
sym3	-0.031432100	-0.024985466	0.018225350	0.003108674
sym3	1342.910204000	1.777957700	576.559067600	1.678590945

Table 5: Continue

Features	Test image 17	Test image 18	Test image 19	Test image 20
rbio3.3	0.029442552	-0.022030664	0.019516232	-1.67E-04000
rbio3.3	7.015318627	0.754303315	706.252169100	0.103678423
rbio3.3	4.452120706	11.249150930	1.032618404	11.590125370
rbio3.5	0.030861590	-0.117185717	0.019461603	0.043234667
rbio3.5	30.546774600	3.403652977	732.025783200	0.171092399
rbio3.5	4.531862745	11.136280730	1.159466912	14.484719670
rbio3.7	0.013671200	-0.173135840	0.020162504	-0.001087088
rbio3.7	60.773976730	0.064235157	498.777475700	0.271255135
rbio3.7	252.683639800	3643.257638000	100.484189400	495.912165900
rbio3.7	4.531862745	11.136280730	1.159466912	14.484719670

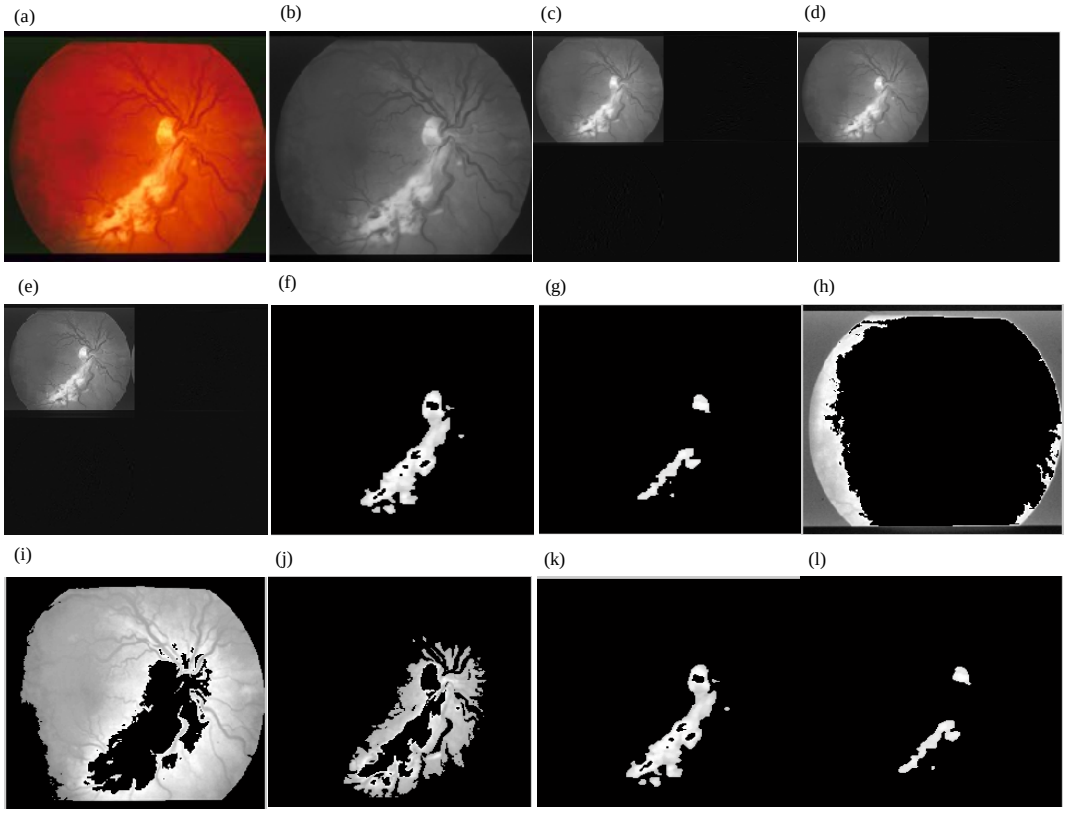

Fig. 3: Abnormal image: a) Input image; b) Gray scale image; c) Daubachies wavelet; d) Symlet; e) Biorthogonal wavelet; f) Abnormal detection 1; g) Abnormal detection 2; h-l) The output of exudates detection

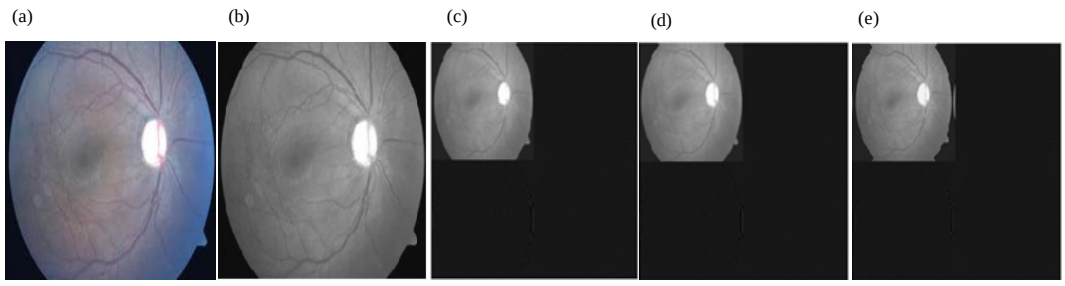

Fig. 4: Gives the output information about the normal image: a) Input image; b) Gray scale image; c) Daubachies wavelet; d) Symlet; e) Biorthogonal wavelet

Table 6: Result comparison between various methods

Classifier name	TN	FN	TP	FP	Accuracy (%)	SI	OF	EF
SVM	8	1	9	2	85	0.857143	0.9	0.2
SMO	9	2	8	1	85	0.842105	0.8	0.1
Random forest	9	1	9	1	90	0.900000	0.9	0.1
PNN	10	1	9	0	95	0.947368	0.9	0.0

Fig. 5: Comparison results

tumor region with manual segmentation but not selected by the method. In a good segmentation, SI and OF should be close to 1 and EF should be close to 0. In Practice, the value of SI is more than 0.7 represented a very good segmentation. About 20 brain images have been taken for evolution. In that 12 images are tumor image and rest of the 8 images are normal image. Table 6 shows the segmentation results obtained from the overall process. Table 6 shows the result comparison between proposed method and earlier methods.

From Fig. 5, it is observed that the proposed model provides very excellent results in classification of glaucomatous image.

CONCLUSION

This research is implemented for glaucomatous image classification using texture features and it will be classified effectively based on neural network. Here, probabilistic neural network is used for classification based on unsupervised leaning using wavelet energy features and target vectors. In addition with an efficient detection of exudates for retinal vasculature disorder analysis is performed. This abnormal region detection was successfully done by using clustering algorithm which is used to provide better segmentation result and performance accuracy. Finally, this system is very useful to diagnose the retinal diseases for early detection vision loss and diabetics. It accurately classifies the image and helps for accurate exudates detection. It results to better performance compared to previous methods.

The proposed image processing and features extraction approach seem to be very promising for the detection of certain pathologies in biomedical images.

RECOMMENDATIONS

For future reseaches, it is recommended to consider a larger set of features and a selection process to identify the most discriminant ones. Furthermore, the DWT-Gabor will be directly compared to the dual-tree complex wavelet, curvelet and contourlet using the same databases and images in order to draw general conclusions. Also, multi-labels classifications will be considered in future works to investigate the discriminative power for each type of pathology. Finally, more experiments on the effect of kernel choice and its parameter on classification accuracy will be investigated. The application of developed algorithm can be extended for failure analysis of mechanical structures made up of metallic and composite material with high resolution images.

REFERENCES

Ahmed, S., K.M. Iftekharuddin and A. Vossough, 2011. Efficacy of texture shape and intensity feature fusion for posterior-fossa tumor segmentation in MRI. IEEE. Trans. Inf. Technol. Biomed., 15: 206-213.

Arivazhagan, S., L. Ganesan and V. Angayarkanni, 2005. Color texture classification using wavelet transform. Proceedings of the 6th International Conference on Computational Intelligence and Multimedia Applications, August 16-18, 2005, Las Vegas, Nevada, pp: 315-320.

Avia-Cervantes J.G., S. Ledezma-Orozco, M. Torres-Cisneros, D. Hernandez-Fusilier, J. Gonzalez-Barbos and A. Salazar-Garibay, 2007. Color texture histograms for natural images interpretation. Proceedings of the 6th Mexican international conference on Artificial Intelligence - Special Session, November 4-10, 2007, Aguas- calientes, Mexico, pp: 131-140.

Bovik, A.C., M. Clark and W.S. Geisler, 1990. Multichannel texture analysis using localized spatial filters. IEEE Trans. Pattern Anal. Machine Intel., 12: 55-73.

Carnapurn Wanderley, J.F. and M.H. Fisher, 2000. Color texture invariants for natural image recognition based on human visual system. Proceedings of the 7th International Conference on Electronics, Circuits and Systems, Vol 1, December 17-20, 2000, Jounieh, Lebanon, pp: 295-298.

Chandrika, S. and K. Nirmala, 2013. Comparative analysis of cdr detection for glaucoma diagnosis. Int. J. Comput. Sci. Appl., 2: 1-9.

Chellappa, R. and S. Chatterjee, 1985. Classification of textures using gaussian markov random fields. IEEE Trans. Acoustics Speech Signal Process, 33: 959-963.

Cheng, K.S., J.S. Lin and C.W. Mao, 1999. Techniques and comparative analysis of neural network systems and fuzzy systems in medical image segmentation. Fuzzy Theor. Syst. Tech. Appl., 3: 973-1008.

Christodoulou, C.I., S.C. Michaelides and C.S. Pattichis, 2006. Multifeature texture analysis for the classification of clouds in satellite imagery. IEEE Trans. Geo Sci. Remote Sens., 41: 2662-2668.

Daubechies, I., 1988. Orthonormal bases of compactly supported wavelets. Commun. Pure Applied Math., 41: 909-996.

Galloway, M.M., 1975. Texture analysis using gray level run lengths. Comput. Graph. Image Process., 4: 172-179.

Gonzalez, R.C. and R.E. Woods, 2010. Texture. In: Digital Image Processing. Gonzalez, R.C. and R.E. Woods (Eds.). 3rd Edn., Pearson, London, UK., ISBN: 0-89252-800-1, pp: 849-861.

Haralick, R.M., 1979. Statistical and structural approaches to texture. Proc. IEEE, 67: 786-804.

Haralick, R.M., K. Shanmugam and I. Dinstein, 1973. Textural features for image classification. IEEE Trans. Syst. Man Cybern., SMC-3: 610-621.

Husoy, J.H., T. Randen and T.O. Gulsrud, 1993. Image texture classification with digital filter banks and transforms. Proceedings of the SPIE's 1993 International Symposium on Optics Imaging and Instrumentation, October 20, 1993, SPIE's, San Diego, California, pp: 260-271.

Jiang, J., P. Trundle and J. Ren, 2010. Medical image analysis with artificial neural networks. Comput. Med. Imaging Graphics, 34: 617-631.

Kandaswamy, U., D.A. Adjeroh, S. Schuckers and A. Hanbury, 2012. Robust color texture features under varying illumination conditions. IEEE Trans. Systerns Man Cybernetics, 42: 58-68.

Khellah, F.M., 2011. Texture classification using dominant neighborhood structure. IEEE. Trans. Image Process., 20: 3270-3279.

Kobayashi, T. and N. Otsu, 2009. Color image feature extraction using color index local auto-correlations. IEEE International Conference on Acoustics, Speech and Signal Processing, April 19-24, 2009, Taipei, China, pp: 1057-1060.

Kurmyshev, E.V. and R.E.S.Yanez, 2005. Comparative experiment with colour texture classifiers using the CCR feature space. Pattern Recognit. Lett., 26: 1346-1353.

Lee, S.Y., K.K. Kim, J.M. Seo, D.M. Kim and H. Chung *et al*., 2004. Automated quantification of retinal nerve fiber layer atrophy in fundus photograph. Proceedings of the 26th Annual International Conference on Engineering in Medicine and Biology Society IEMBS'04, September 1-5, 2004, IEEE, San Francisco, California, ISBN: 0-7803-8439-3, pp: 1241-1243.

Lepisto, L., I. Kunttu, J. Autio and A. Visa, 2003. Classification method for colored natural textures using gabor filtering. Proceedings of the 12th International Conference on Analysis and Processing, September 17-19, 2003, Mantova, Italy, pp: 397-401.

Liao, S., M.W.K. Law and A.C.S. Chung, 2009. Dominant local binary patterns for texture classification. IEEE Trans. Pattern Anal. Mach. Intell., 18: 1107-1118.

Rajaei, A. and L. Rangarajan, 2011. Wavelet features extraction for medical image classification. Int. J. Eng. Sci., 4: 131-141.

Tamilpavai, G. and S.T. Selvi, 2012. Multiple representations of perceptual features for texture classification and retrieval. Int. J. Comput. Appl., 48: 5-11.

Yang, H.Y., X.Y. Wang, X.Y. Zhang and J. Bu, 2012. Color texture segmentation based on image pixel classification. Eng. Appl. Artif. Intell., 25: 1656-1669.

Zhang, H., A.C. Berg, M. Maire and J. Malik, 2006. SVM-KNN: Discriminative nearest neighbor classification for visual category recognition. Proceedings of the IEEE Computer Society Conference on Computer Vision and Pattern Recognition-Volume 2, June 17-22, 2006 Washington, DC, USA., pp: 2126-2136.

Zheng, L., J. Zhang and Y. Luo, 2006. Colour matching in color remote sensing image. Proceedings of the First International Multi-Symposiums on Computer and Computational Sciences, Vol 1, June 20-24, 2006, Hangzhou, China, pp: 303-306.

Zheng, Q. and E.Q. Dong, 2013. Narrow band active contour model for local segmentation of medical and texture images. Acta Automatica Sin., 39: 21-30.